Article

Not peer-reviewed version

Characterization of As-Synthesized PANI/CeO_2 Nanocomposite Films for Enhanced Anti-corrosion Applications

Ahmad Alsaad *, Mohannad Al-Hmoud, Taha Rababah, MOHAMMAD MARASHDEH, Mamduh J. Aljaafreh, Sharif Abu Alrub, Ayed M. Binzowaimil, Ahmad Telfah

Posted Date: 16 February 2024

doi: 10.20944/preprints202402.0894.v1

Keywords: corrosion protection; protonated polyaniline (PANI); cerium dioxide (CeO_2); optical bandgap energy; electrical conductivity

Article

Characterization of As-Synthesized PANI/CeO_2 Nanocomposite Films for Enhanced Anti-Corrosion Applications

Ahmad M. Alsaad [a,d,*], Mohannad Al-Hmoud [b], Taha M. Rababah [e], Mohammad W. Marashdeh [b], Mamduh J. Aljaafreh [b], Sharif Abu Alrub [b], Ayed Binzowaimil [b] and Ahmad Telfah [c,d]

[a] Department of Physics, Jordan University of Science and Technology, P.O. Box 3030, Irbid 22110, Jordan
[b] Department of Physics, College of Science, Imam Mohammad Ibn Saud Islamic University (IMSIU), P.O. Box 90950, Riyadh, 11623, Saudi Arabia
[c] Nanotechnology Center, The University of Jordan, 11942, Amman, Jordan
[d] Department of Physics, University of Nebraska at Omaha, Omaha NE-68182, USA
[e] Department of Nutrition and Food Technology, Faculty of Agriculture, Jordan University of Science and Technology, P.O. Box 3030, Irbid 22110, Jordan
* Correspondence: alsaad11@just.edu.jo or amalsaad@unomaha.edu; Tel.: +962 2 720100 Ext: 23422, Fax: +962 2 7201071

Abstract: This study introduces a novel nanocomposite coating composed of PANI/CeO_2 nanocomposite films, aimed at addressing corrosion protection needs. Analysis through FTIR spectra and XRD patterns confirms the successful formation of the nanocomposite films. Notably, the PANI/CeO_2 nanocomposite films exhibit a hydrophilic nature. The bandgap energy of the PANI composite film measures at 3.74 eV, while the introduction of CeO_2 NPs into the PANI matrix reduces the bandgap energy to 3.67 eV. Furthermore, the electrical conductivity of the PANI composite film is observed to be 0.40 $S.cm^{-1}$, with the incorporation of CeO_2 NPs leading to an increase in electrical conductivity to 1.07 $S.cm^{-1}$. To evaluate its efficacy, electrochemical measurements were conducted to assess the corrosion protection performance. Results indicate a high protection efficiency of 92.25% for the PANI/CeO_2 nanocomposite film.

Keywords: Corrosion protection; Protonated Polyaniline (PANI); Cerium dioxide (CeO_2); Optical bandgap energy; Electrical conductivity

Introduction

The corrosion of metals has been one of the essential problems that faced scientific and industrial societies. There is a lot of attention from these societies to develop long-life corrosion protection coating [1,2].

Polyaniline (PANI) is one of the most promising conductive polymers that is used in the fabrication of corrosion protective coating due to its good redox recyclability, variable electrical conductivity, and good environmental stability [3]. PANI nanocomposites is used as an exhilarating technique to enhance the corrosion protection performance significantly. This could be attributed to the fact that PANI composite coating triggers the redox action in an extensive range of pH values and increases corrosion protection performance [4–6].

Several works have elaborated on techniques to enhance the corrosion protection of PANI coating by introducing ceria nanoparticles (CeO_2 NPs) [7]. M. Hosseini and K. Aboutalebi [8] reported that incorporating epoxy coating with CeO_2@PANI@MBT significantly enhances the corrosion protection performance of mild steel substrates. In addition, M. Montemor et al. [9] and L. Calado et al. [10] reported that modifying silane film and siloxane film by CeO_2NPs enhances corrosion protection and film stability. Y. Lei et al. [11] concluded that PANI/CeO_2 nanocomposite coating could be a potential candidate to improve the protection performance of the epoxy coating on carbon steel.

In our research, we introduce an innovative nanocomposite coating comprising PANI/CeO_2 nanocomposite films tailored for corrosion protection applications. We delve into a comprehensive

 doi:10.20944/preprints202402.0894.v1

analysis of the chemical, structural, morphological, and surface wettability properties of these PANI/CeO_2 nanocomposite films. Furthermore, we explore the impact of incorporating CeO_2 into the PANI matrix on the thermal stability of the composite. Detailed investigations into the optical and electrical properties, including absorption coefficient, bandgap energy, and electrical conductivity, provide valuable insights. Additionally, we conduct a thorough examination of the corrosion protection performance of PANI/CeO_2 nanocomposite films across varying temperatures, shedding light on their efficacy in real-world conditions.

2. Methods

2.1. Materials

The samples used in this study were prepared from the following materials: Polyaniline (PANI, emeraldine base, 50,000 g/mol), camphor sulfonic acid (CSA, 232.30 g/mol), N-Methyl-2-Pyrrolidone (NMP, 99.133 g/mol), Ferric oxide nanoparticles (Fe_3O_4NPs, 50-100 nm particle size), cerium dioxide nanoparticles (CeO_2NPs of size less than 50 nm). All the materials were purchased from Sigma Aldrich (formally Millipore Sigma).

2.2. Synthesis technique

To prepare PANI composite solution, 0.5 g Polyaniline and 0.12 g CSA were dissolved in 100 mL NMP. The mixture was subjected to a vigorous magnetic stirring overnight at 55 °C. To obtain a homogenous solution,

PANI composite solution was sonicated at 55 °C for three hours. Moreover, solution mixed method was utilized to synthesize PANI/CeO_2 NPs nanocomposite solutions. Under magnetic stirring for five hours, five wt.% of CeO_2 was added separately to PANI composite solution at room temperature.

The resulting PANI/CeO_2 nanocomposite solutions were sonicated for 3 hours at room temperature. To obtain the desired investigated structures, we employed casting technique to deposit PANI and PANI/CeO_2 nanocomposite films on ITO and steel substrates. To prevent any modifications on the surface morphology and to ensure complete drying of all residuals, the deposited films were dried at 40 °C at ambient condition overnight

2.2. Characterization methods

The chemical, structural, and morphological characterizations were conducted using FTIR microscope (HYPERION 3000 Bruker), XRD (Malvern Panalytical Ltd.), and SEM micrographs (Quanta FEG 450), respectively. Thermogravimetric analysis (TGA, NETZSCH) was utilized to investigate thermal stability of the as prepared PANI and PANI/CeO_2 thin films. A UV–Vis spectrophotometer (Hitachi U-3900H) with a total internal sphere was used to obtain and interpret the optical properties. A four-point probe (Microworld Inc.) hocked up to a high-resolution Keithley 2450 Sourcemeter was employed to measure and interpret the electrical conductivity. The corrosion protection performance was investigated using the polarization method.

3. Results and Discussion

The chemical, structural, and morphological characteristics of PANI and PANI/CeO_2 nanocomposite films were investigated and interpreted using the FTIR absorbance spectra (Figure 1), XRD patterns (Figure 2), SEM images and water contact angle measurements (Figure 3). Figure 1 displays the FTIR spectra of PANI and PANI/CeO_2 nanocomposite films in 500-4000 cm^{-1} spectral range. For protonated PANI film, the C = N iminoquinone vibrational band appears at 660 cm^{-1} [12]. Additionally, the absorption band at 825 cm^{-1} is assigned to the aromatic rings. This is a strong evidence of the formation of the polymer [13]. The vibrational band that appears at 950 cm^{-1} refers to $-SO_3H$ group, ratifying the PANI protonation with CSA. Furthermore, the in-plane C - H bending vibrations within the quinoid unit (N = Q = N) appear at 1125 cm^{-1}. Also, the aromatic C − N stretching vibrations appear in the 1300-1500 cm^{-1} spectral range [14]. The C - N stretching vibrations inside benzenoid (N - B - N) and quinoid (N = Q = N) rings are located at 1541 and 1651 cm^{-1}, respectively. The absorption bands beyond 3000 cm^{-1} indicate the N - H stretching vibrations [14]. Incorporation of CeO_2 NPs into the protonated PANI films strongly moved the vibrational bands to the higher

 doi:10.20944/preprints202402.0894.v1

region of the spectrum. This strong shift is mainly attributed to the difference in the electronegativity between CeO_2 NPs and the PANI molecules.

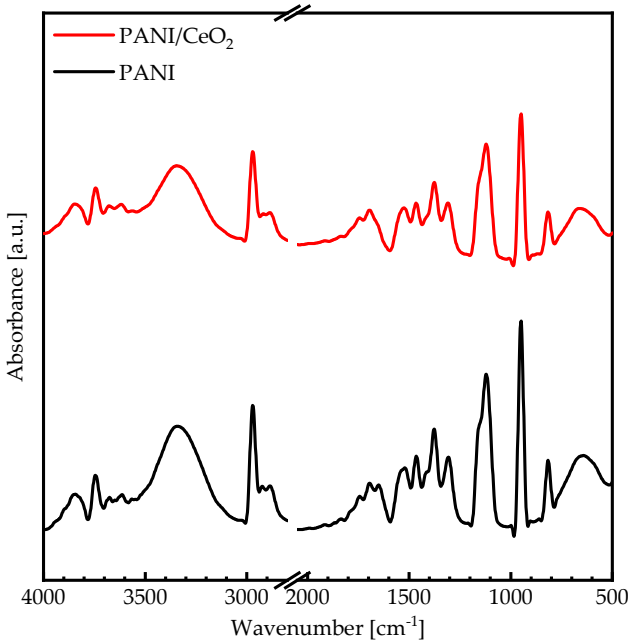

Figure 1. The FTIR spectra of PANI and PANI/CeO_2 nanocomposite films in the 500-4000 cm^{-1} spectral range.

Figure 2 shows the XRD patterns of PANI and PANI/CeO_2 nanocomposite films in the 10°-50° angular range. Clearly, the crystal structure of PANI is mainly determined by the synthesis conditions and the type of the protonic acid [15]. Protonated PANI film shows diffraction peaks at 14.97°, 20.72°, and 25.38° corresponding to (011), (001), and (110) diffraction crystallographic planes [16]. Additionally, a diffraction peak located at 27.86° associated with the CSA, confirming the protonation of PANI. The semi-crystalline protonated PANI with CSA has two phases. Namely, the phase in which the polymer chains are ordered (crystalline phase), and the phase in which the polymer chains are randomly distributed (amorphous phase) [17]. On the contrary, the protonated PANI/CeO_2 nanocomposite film exhibits an amorphous phase.

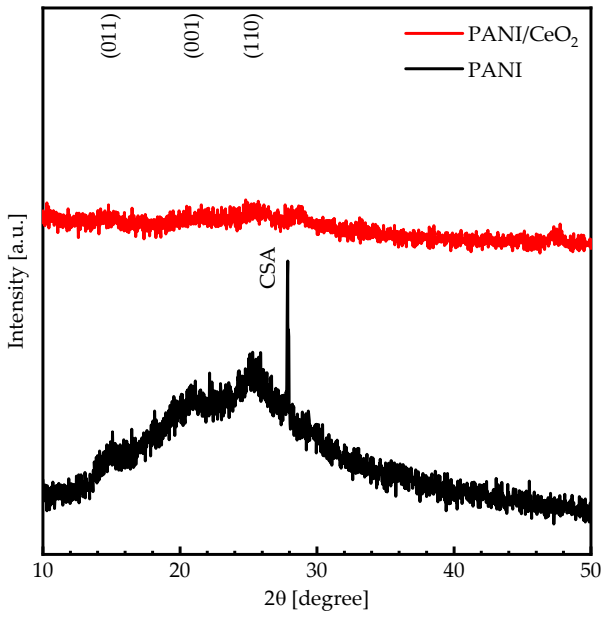

Figure 2. The XRD patterns of PANI and PANI/CeO_2 nanocomposite films in a diffraction angle range of 10°-50°.

Preprints.org (www.preprints.org) | NOT PEER-REVIEWED | Posted: 16 February 2024 doi:10.20944/preprints202402.0894.v1

Figure 3 demonstrates the 1 μm scaled-SEM micrographs and water contact angle (WCA) measurements for PANI and PANI/CeO_2 nanocomposite films. As can be clearly seen, the protonated PANI film shows a rod-like shape with a WCA of 38°, indicating that the protonated PANI film has a hydrophilic nature (Figure 3a). Adding CeO_2 NPs into the PANI matrix leads to the decrease of the grain sizes as well as the WCA (24°) (Figure 3b).

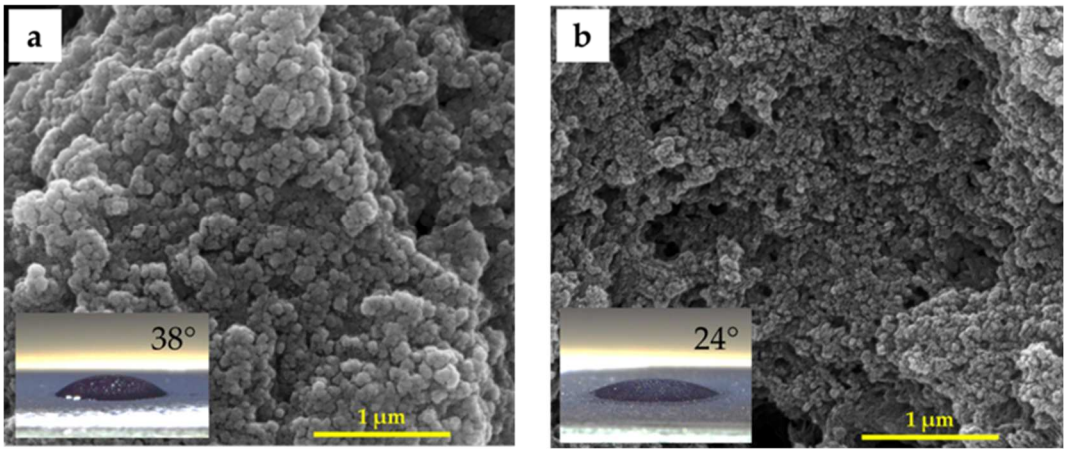

Figure 3. SEM images of **(a)** PANI and **(b)** PANI/CeO_2 nanocomposite films at 1 μm scale.

The absorption spectra of PANI and PANI/CeO_2 nanocomposite films were investigated. The absorption coefficient can be expressed as, $\alpha = (1/d)\ln\left((1-R)/T\right)$ [18,19]. The parameters T, R, and d stands for the transmittance, reflectance, and film thickness, respectively. The parameter α exhibits a sudden decrease from 0.01 to 0.003 as incident wavelength increases from 300 to 350 nm. Beyond $\lambda = 350\,nm$, it attains a constant vales as demonstrated by Figure 4. The vibration band appears between 400 and 480 nm is related to the superposition of the π-π* transition within the benzoin ring with the confined polarons (polaron-π*) transition [20]. Introducing CeO_2 NPs into the PANI composite matrix increases α in the visible region and shifts the absorption edge into the red region. The bandgap energy of both PANI and PANI/CeO_2 nanocomposite films was calculated using the Tauc plot method[21,22]. The bandgap energy of the PANI composite film was calculated to be 3.74 eV. Introducing CeO_2 NPs into the PANI matrix decreases the bandgap energy to 3.67 eV.

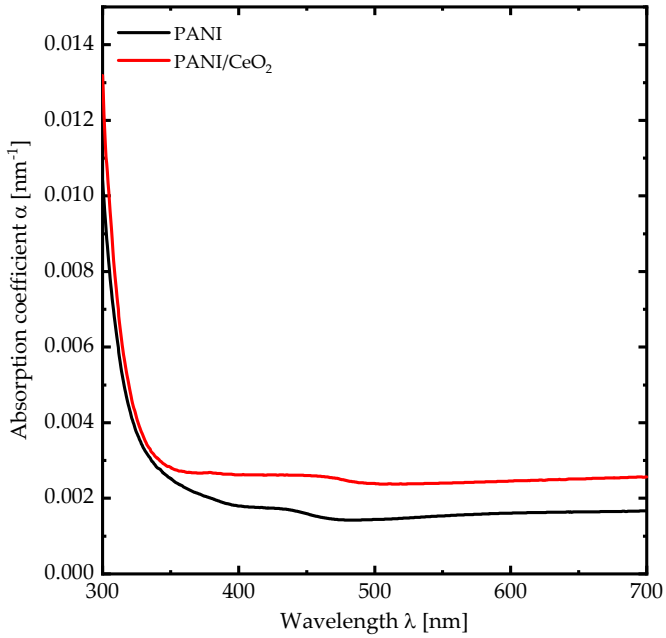

Figure 4. Absorption coefficient spectra of PANI and PANI/CeO_2 nanocomposite films.

 doi:10.20944/preprints202402.0894.v1

The two PANI and PANI/CeO_2 nanocomposite thin films samples are characterized electrically By measuring electrical conductivity using a 4-point probe at 12 distinct points. The measured electrical conductivity of the PANI composite film is found to be 0.40 $S.cm^{-1}$. The considerably large conductivity could be attributed to the strong acid-doping of CSA, which provides additional charge carriers by protonating the imine nitrogen of the PANI backbone [23]. Incorporation of CeO_2NPs into the PANI composite film more than doubles the electrical conductivity to 1.07 $S.cm^{-1}$. To obtain a deeper insight into electrical conductivity values, the electrical conductivity maps (1 cm x 1 cm) of PANI and PANI/CeO_2 nanocomposite films are measured and presented in Figure 5. Careful examination of (Figure 5a) indicates significant variation of the conductivity across PANI composite film caused by substantial surface morphology alterations as well as the quality and conditions of the growth process. Introducing CeO_2NPs into the PANI composite matrix considerably changes the conductivity distribution. This could be attributed to the dispersion of each type of nanoparticle in the PANI matrix (Figure 5b).

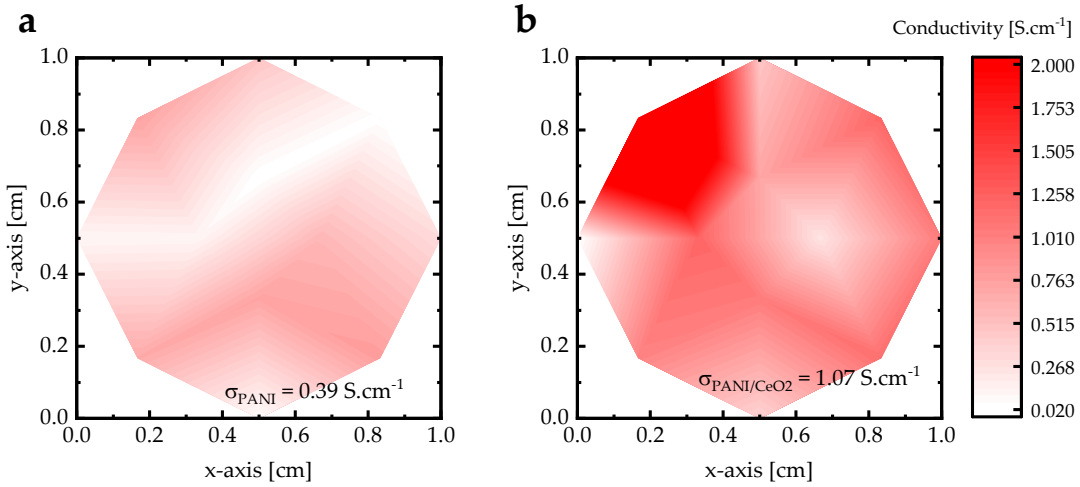

Figure 5. The electrical conductivity maps of **(a)** PANI and **(b)** PANI/CeO_2 nanocomposite films.

Polarization method was used to elucidate the corrosion rate of PANI and PANI/CeO_2 nanocomposite films. The corrosion test was evaluated in 3.5 wt.% NaCl solution at a temperature of 298 K (Figure 6a). The corrosion potential (E_{corr}) and corrosion current (I_{corr}) were evaluated at the junction where the tangent of the anodic and cathodic polarization curves intersect. The corrosion rate of the nanocomposite films can be calculated using $CR = kMI_{\mathrm{corr}}/\rho_m$ [24,25], where k is a parameter equals to 3268.5 mol/A, M stands for the molecular weight of carbon steel, ρ_m is the density of carbon steel. The parameters E_{corr}, I_{corr} and CR of electrochemical measurements are tabulated in Table 1. It can be seen that the corrosion rate of PANI-coated carbon steel is lower than the corrosion rate of bare carbon. In addition, incorporating PANI with CeO_2 decreases the corrosion rate. The lowest corrosion rate is found for PANI/CeO_2 nanocomposite films (0.112 mm/year). The protection efficiency ($\eta_{PROT}(\%)$) can be calculated using $\eta_{PROT}(\%) = (i^0_{corr} - i^{coat}_{corr})/i^0_{corr} \times 100\%$, where the parameter i^0_{corr} represents corrosion current of bare carbon steel and i^{coat}_{corr} stands for the corrosion current of the nanocomposite coated carbon steel [26]. The higher protection efficiency was obtained for PANI/CeO_2 nanocomposite films with a value of 92.25%.

 doi:10.20944/preprints202402.0894.v1

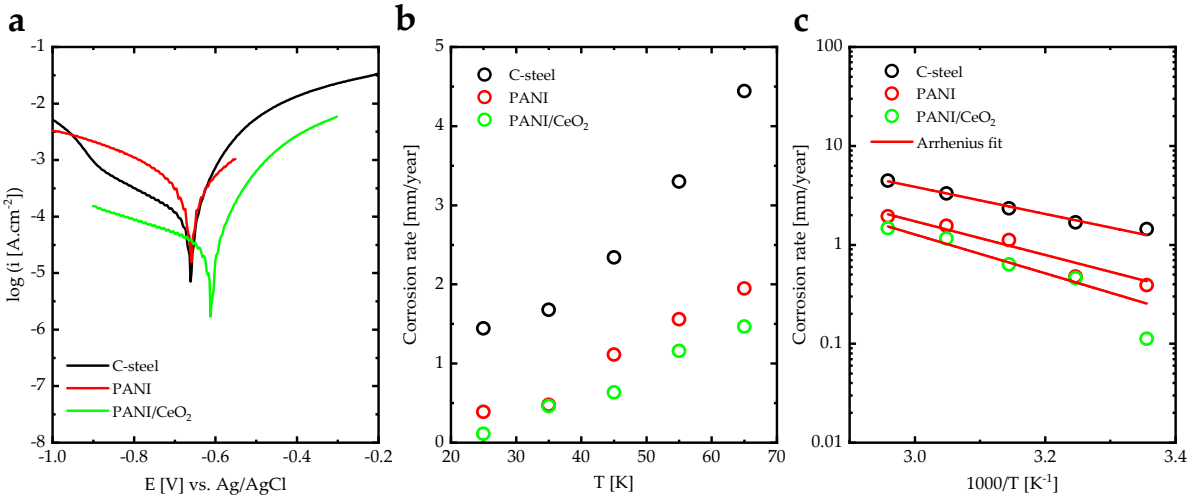

Figure 6. (a) Tafel curve of carbon steel coated with PANI and PANI/CeO_2 nanocomposite films at 298 K, **(b)** corrosion rate of carbon steel coated with PANI and PANI/CeO_2 nanocomposite films as a function of temperature [K], and **(c)** corrosion rate of carbon steel coated with PANI and PANI/CeO_2 nanocomposite films as a function of 1000/temperature [K] fitted to Arrhenius function.

Table 1. Electrochemical parameters values for carbon steel coated with PANI and PANI/CeO_2 nanocomposite films at 298 K values calculated from Tafel plots.

	C-Steel	**PANI**	**PANI/CeO_2**
CR [mm/year]	1.445	0.390	0.112
η_{PROT}(%)	--	72.90	92.25
E_a [eV]	0.27	0.34	0.39

The corrosion rate of PANI and PANI/CeO_2 nanocomposite films were calculated in the 298-338 K temperature range (Figure 6b). As the temperature of the electrochemical reaction is increased, the corrosion rate for all nanocomposite films increases. This increase is a direct consequence of the enhanced electrochemical reaction rates as well as the increase in the kinetic energy of the molecules in the electrolyte solution. Therefore, the diffusion rate of the molecules is significantly increased. To clarify the thermal activated processes of the corrosion reactions [27], the corrosion rates of PANI and PANI/CeO_2 nanocomposite films versus the reciprocal of temperature (1000/T[K]) are illustrated in Figure 6c. As can be clearly seen, corrosion rates exhibit Arrhenius-like behavior ($CR = CR_0 \exp(-E_a/K_BT)$) [28]. This means that the corrosion rate of bare carbon steel and carbon steel coating by PANI, PANI/ZrO_2, PANI/Fe_3O_4, and PANI/(ZrO_2-Fe_3O_4) nanocomposite films are thermally activated. The activation energies deduced by Arrhenius fitting are tabulated in Table 1. Obviously, the highest activation energy is obtained for PANI/CeO_2 nanocomposite film. Thus, the effect of temperature on the corrosion rate of PANI/CeO_2 nanocomposite film is more pronounced than for other investigated samples.

Figure 7 illustrates the effect of coating on the Nyquist and the Bode plots of PANI and PANI/CeO_2 nanocomposite films immersed in 3.5 wt.% NaCl at 298 K. In the Nyquist plot, the curves have single capacity arcs with large radii for PANI/CeO_2 nanocomposite films compared to bare carbon steel and PANI film (Figure 7a), indicating the resistance of these nanocomposites is very high. The coating has an exceptional physical barrier influence on the electrolyte. The Z value in the Bode diagram at 0.1 Hz increases from 652 $\Omega.cm^{-2}$ for bare steel to 1900 $\Omega.cm^{-2}$ for PANI/CeO_2 nanocomposite film. Thus, coating the carbon steel by PANI/CeO_2 nanocomposite film enhances the corrosion resistance (Figure 7b).

 doi:10.20944/preprints202402.0894.v1

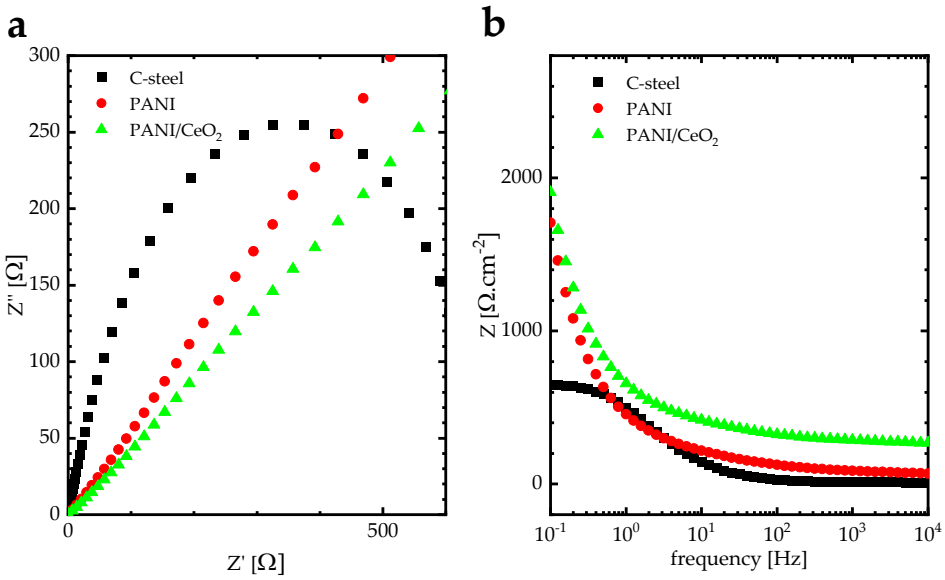

Figure 7. (a) Nyquist and **(b)** Bode plots of carbon steel coated with PANI and PANI/CeO_2 nanocomposite films at 298 K.

4. Conclusions

This work reports the results on a novel nanocomposite coating of PANI/CeO_2 nanocomposite film for corrosion protection applications. FTIR spectra and XRD patterns confirm the formation of the nanocomposite films. Water contact angle measurements confirm that PANI/CeO_2 nanocomposite film has a hydrophilic nature. Therefore, the films are capable of interacting with water through hydrogen bonding. Optical measurements reveal that bandgap energy of the PANI composite film is 3.74 eV. Introducing CeO_2 NPs into the PANI matrix decreases the bandgap energy to 3.67 eV. Consequently, bandgap engineering in PANI/CeO_2 nanocomposite film could be a powerful technique for the design of new materials and devices based on this novel material. In addition, band diagrams with continuous bandgap variations can be generated in heterojunctions designed from this novel material and fabricated using techniques such as molecular beam epitaxy. The electrical conductivity measurements reveal that PANI composite film exhibits an electrical conductivity of 0.40 $S.cm^{-1}$. Introducing CeO_2 NPs into the PANI composite film increases the electrical conductivity by more than two-fold to 1.07 $S.cm^{-1}$. The corrosion protection performance was investigated using electrochemical measurements. The protection efficiency of PANI/CeO_2 nanocomposite film is 92.25%. In general, the efficiency of an inhibitor increases with an increase in inhibitor concentration. Obtaining excellent inhabitation for incorporating 5 wt.% of CeO_2 in PANI nanocomposite films is very promising for corrosion protection applications.

Author Contributions: Conceptualization: Ahmad Alsaad, Mohannad Al-Hmoud, Ahmad D. Telfah; **Methodology**: Ahmad Alsaad, Mohannad Al-Hmoud, Mohammad W. Marashdeh, Ahmad D. Telfah; **Investigation**: Ahmad M. Alsaad, Mohannad Al-Hmoud, Taha M. Rababah, Mohammad W. Marashdeh, Mamduh J. Aljaafreh, Sharif Abu Alrub , Ayed Binzowaimil , and Ahmad Telfah; **Data curation**: Ahmad M. Alsaad, Mohannad Al-Hmoud, Taha M. Rababah, Mohammad W. Marashdeh, Mamduh J. Aljaafreh, Sharif Abu Alrub , Ayed Binzowaimil , and Ahmad Telfah; **Formal analysis:** Ahmad Alsaad, Mohannad Al-Hmoud, Ahmad D. Telfah; **Writing – original draft**: Ahmad M. Alsaad, Mohannad Al-Hmoud, Taha M. Rababah, Mohammad W. Marashdeh, Mamduh J. Aljaafreh, Sharif Abu Alrub, Ayed Binzowaimil, and Ahmad Telfah; **Writing – review & editing**: Ahmad M. Alsaad, Mohannad Al-Hmoud, Taha M. Rababah, Mohammad W. Marashdeh, Mamduh J. Aljaafreh, Sharif Abu Alrub, Ayed Binzowaimil, and Ahmad Telfah; **Funding acquisition:** Ahmad Alsaad, Mohannad Al-Hmoud; **Project administration:** Ahmad Alsaad, Mohannad Al-Hmoud; **Resources:** Ahmad M. Alsaad, Mohannad Al-Hmoud, Taha M. Rababah, Mohammad W. Marashdeh, Mamduh J. Aljaafreh, Sharif Abu Alrub, Ayed Binzowaimil, and Ahmad Telfah; **Supervision**: Ahmad Alsaad, Mohannad Al-Hmoud, Ahmad D. Telfah; **Validation:** Ahmad M. Alsaad, Mohannad Al-Hmoud, Taha M. Rababah, Mohammad W. Marashdeh, Mamduh J. Aljaafreh, Sharif Abu Alrub , Ayed Binzowaimil , and Ahmad Telfah; **Visualization:** Ahmad M. Alsaad, Mohannad Al-Hmoud, Taha M. Rababah, Mohammad W.

Marashdeh, Mamduh J. Aljaafreh, Sharif Abu Alrub , Ayed Binzowaimil , and Ahmad Telfah. All authors have read, reviewed and agreed to the submitted version of the manuscript.

Data Availability Statement: The data that support the findings of this study are available on request from the corresponding author, [Ahmad Alsaad].

Conflicts of Interest: All the authors of this manuscript declare no conflict of interest.

Data availability: Unprocessed data were available upon request from the corresponding author.

Acknowledgments : This work was supported and funded by the Deanship of Scientific Research at Imam Mohammad Ibn Saud Islamic University (IMSIU) (grant number IMSIU-RP23104).

References

1. B. Ramezanzadeh, M. M. Moghadam, N. Shohani, and M. Mahdavian, "Effects of highly crystalline and conductive polyaniline/graphene oxide composites on the corrosion protection performance of a zinc-rich epoxy coating," *Chemical Engineering Journal,* vol. 320, pp. 363-375, 2017.
2. N. N. Taheri, B. Ramezanzadeh, M. Mahdavian, and G. Bahlakeh, "In-situ synthesis of Zn doped polyaniline on graphene oxide for inhibition of mild steel corrosion in 3.5 wt.% chloride solution," *Journal of industrial and engineering chemistry,* vol. 63, pp. 322-339, 2018.
3. T. S. Natarajan, C.-H. Tsai, H.-L. Huang, K.-S. Ho, I. Lin, and Y.-F. Wang, "Fabrication of polyaniline coated plasma modified polypropylene filter for antibioaerosol application," *Aerosol and Air Quality Research,* vol. 16, pp. 1911-1921, 2016.
4. G. Qiu, A. Zhu, and C. Zhang, "Hierarchically structured carbon nanotube–polyaniline nanobrushes for corrosion protection over a wide pH range," *Rsc Advances,* vol. 7, no. 56, pp. 35330-35339, 2017.
5. B. Ramezanzadeh, G. Bahlakeh, and M. Ramezanzadeh, "Polyaniline-cerium oxide (PAni-CeO2) coated graphene oxide for enhancement of epoxy coating corrosion protection performance on mild steel," *Corrosion Science,* vol. 137, pp. 111-126, 2018.
6. Y. Hayatgheib, B. Ramezanzadeh, P. Kardar, and M. Mahdavian, "A comparative study on fabrication of a highly effective corrosion protective system based on graphene oxide-polyaniline nanofibers/epoxy composite," *Corrosion Science,* vol. 133, pp. 358-373, 2018.
7. M. Abdeslam, B. Hichem, and H. Youcef, "Synthesis of polyaniline/CeO2 nanocomposites as inhibitor coating on zinc: Evaluation of the corrosion behaviour," in *International Conference on Scientific and Innovative Studies*, 2023, vol. 1, no. 1, pp. 282-288.
8. M. G. Hosseini and K. Aboutalebi, "Enhancement the anticorrosive resistance of epoxy coatings by incorporation of CeO2@ polyaniline@ 2-mercaptobenzotiazole nanocomposite," *Synthetic Metals,* vol. 250, pp. 63-72, 2019.
9. M. Montemor and M. Ferreira, "Cerium salt activated nanoparticles as fillers for silane films: Evaluation of the corrosion inhibition performance on galvanised steel substrates," *Electrochimica Acta,* vol. 52, no. 24, pp. 6976-6987, 2007.
10. L. M. Calado, M. G. Taryba, M. J. Carmezim, and M. F. Montemor, "Self-healing ceria-modified coating for corrosion protection of AZ31 magnesium alloy," *Corrosion Science,* vol. 142, pp. 12-21, 2018.
11. Y. Lei *et al.*, "Polyaniline/CeO2 nanocomposites as corrosion inhibitors for improving the corrosive performance of epoxy coating on carbon steel in 3.5% NaCl solution," *Progress in Organic Coatings,* vol. 139, p. 105430, 2020.
12. S. Daikh, F. Zeggai, A. Bellil, and A. Benyoucef, "Chemical polymerization, characterization and electrochemical studies of PANI/ZnO doped with hydrochloric acid and/or zinc chloride: differences between the synthesized nanocomposites," *Journal of Physics and Chemistry of Solids,* vol. 121, pp. 78-84, 2018.
13. M. V. Kulkarni, A. K. Viswanath, R. Marimuthu, and T. Seth, "Spectroscopic, transport, and morphological studies of polyaniline doped with inorganic acids," *Polymer Engineering & Science,* vol. 44, no. 9, pp. 1676-1681, 2004.
14. H. Chamroukhi *et al.*, "Optical and structural properties enhancement of hybrid nanocomposites thin films based on polyaniline doped with Zinc Oxide embedded in bimodal mesoporous silica (ZnO@ SiOX) nanoparticles," *Optical Materials,* vol. 84, pp. 703-713, 2018.
15. M. A. C. Mazzeu, L. K. Faria, A. d. M. Cardoso, A. M. Gama, M. R. Baldan, and E. S. Gonçalves, "Structural and morphological characteristics of polyaniline synthesized in pilot scale," *Journal of Aerospace Technology and Management,* vol. 9, pp. 39-47, 2017.
16. R. S. Diggikar, S. P. Deshmukh, T. S. Thopate, and S. R. Kshirsagar, "Performance of polyaniline nanofibers (PANI NFs) as PANI NFs-silver (Ag) nanocomposites (NCs) for energy storage and antibacterial applications," *ACS Omega,* vol. 4, no. 3, pp. 5741-5749, 2019.

17. S. Bhadra and D. Khastgir, "Determination of crystal structure of polyaniline and substituted polyanilines through powder X-ray diffraction analysis," *Polymer Testing,* vol. 27, no. 7, pp. 851-857, 2008.
18. I. Dhahri *et al.*, "Optical and structural properties of ZnO NPs and ZnO–Bi2O3 nanocomposites," *Ceramics International,* vol. 48, no. 1, pp. 266-277, 2022.
19. A. Hassanien *et al.*, "Effect of fast annealing on structural characteristics and optical properties of Cu2ZnSnS4 absorber films deposited by doctor-blade technique," *Journal of Nanoelectronics and Optoelectronics,* vol. 14, no. 10, pp. 1394-1400, 2019.
20. Q. M. Al-Bataineh, V. Shpacovitch, D. Sadiq, A. Telfah, and R. Hergenröder, "Surface Plasmon Resonance Sensitivity Enhancement Based on Protonated Polyaniline Films Doped by Aluminum Nitrate," *Biosensors,* vol. 12, no. 12, p. 1122, 2022.
21. A. S. Hassanien, R. Neffati, and K. Aly, "Impact of Cd-addition upon optical properties and dispersion parameters of thermally evaporated CdxZn1-xSe films: discussions on bandgap engineering, conduction and valence band positions," *Optik,* vol. 212, p. 164681, 2020.
22. A. Hassanien *et al.*, "Investigation of structural, electrical and optical properties of chitosan/fullerene composites," *Materials Research Express,* vol. 6, no. 12, p. 125304, 2019.
23. M. Al-Gharram, I. Jum'h, A. Telfah, and M. Al-Hussein, "Highly crystalline conductive electrodeposited films of PANI-CSA/CoFe2O4 nanocomposites," *Colloids and Surfaces A: Physicochemical and Engineering Aspects,* vol. 628, p. 127342, 2021.
24. S. Yang, S. Zhu, and R. Hong, "Graphene oxide/polyaniline nanocomposites used in anticorrosive coatings for environmental protection," *Coatings,* vol. 10, no. 12, p. 1215, 2020.
25. Y.-T. Lin *et al.*, "Improvement of mechanical properties and anticorrosion performance of epoxy coatings by the introduction of polyaniline/graphene composite," *Surface and Coatings Technology,* vol. 374, pp. 1128-1138, 2019.
26. A. A. Al-Amiery, A. B. Mohamad, A. A. H. Kadhum, L. M. Shaker, W. N. R. W. Isahak, and M. S. Takriff, "Experimental and theoretical study on the corrosion inhibition of mild steel by nonanedioic acid derivative in hydrochloric acid solution," *Scientific Reports,* vol. 12, no. 1, p. 4705, 2022.
27. H. Almashhadani, "Synthesis of a CoO–ZnO nanocomposite and its study as a corrosion protection coating for stainless steel in saline solution," *Int. J. Corros. Scale Inhib,* vol. 10, no. 3, pp. 1294-306, 2021.
28. A. Telfah, A. Kalfe-Yildiz, Q. M. Al Bataineh, I. Jum'h, C. J. Tavares, and R. Hergenröder, "Thermal-dependent morphological evolution effect on ion transportation in polyethylene oxide films," *Polymer,* vol. 288, p. 126440, 2023.
29.